Sustainable Energy & Fuels

ROYAL SOCIETY OF CHEMISTRY

PAPER

View Article Online
View Journal | View Issue

Cite this: *Sustainable Energy Fuels*, 2023, **7**, 1265

Conversion of CO_2 to gasoline over tandem Fe/C and HZSM-5 catalysts†

Ke Jin,[ac] Chengyan Wen,[b] Qian Jiang,[a] Xiuzheng Zhuang,[b] Lungang Chen,[b] Longlong Ma,[b] Chenguang Wang *[ac] and Qi Zhang *[b]

Thermal catalytic conversion of CO_2 to produce high-value gasoline is a promising and sustainable way to deal with greenhouse gases and alleviate the energy crisis and environmental problems. Although significant efforts have been invested in this area, the active catalysts required to achieve high gasoline space time yields remain a bottleneck in the process. Herein, we provided an easy-to-prepare Fe/C catalyst coupled with HZSM-5 as a tandem catalyst, showing a surprisingly high gasoline space-time yield of 91.2 $\mu mol_{CO_2}\ g_{Fe}^{-1}\ s^{-1}$. The catalyst contained three active sites (Fe_3O_4, Fe_5C_2 and acid sites) that could synergistically catalyze a tandem reaction. Tandem catalysts loaded in layers could better exploit the activity of the three sites. The highly selective light olefins produced on the Fe/C catalyst could be converted to gasoline on downstream HZSM-5. More promisingly, the stable and excellent CO_2 hydrogenation to light olefin activity of the Fe/C catalyst and the excellent anti-carbon deposition ability of HZSM-5 resulted in no significant deactivation of the tandem catalyst over 180 h. Overall, the present work provides a green and efficient catalyst for the conversion of CO_2 to gasoline, which will benefit the sustainability of the field in the near future.

Received 12th November 2022
Accepted 10th January 2023

DOI: 10.1039/d2se01567f

rsc.li/sustainable-energy

1. Introduction

In recent years, the combustion of fossil fuels such as coal, oil and natural gas has produced a large amount of CO_2, resulting in increasingly serious environmental problems due to the greenhouse effect.[1–3] At the same time, the depletion of fossil resources also led to a gradual increase in oil prices.[4] Thermal catalytic upgrading of CO_2 into gasoline fuel (C_5–C_{11} range hydrocarbons) not only helps to reduce CO_2 emissions, but also provides valuable fuel, thereby improving energy security.[5,6] The conversion of CO_2 to gasoline is mainly achieved by the oxygenated intermediate or olefin intermediate route.[7] The former usually occurs over a tandem catalyst consisting of metal oxides (Zn, ln, Zr, *etc.*) and acidic zeolites,[8–10] while the latter occurs over a tandem catalyst consisting of Fischer–Tropsch catalysts (Fe, Co, Cu, *etc.*) and acidic zeolites.[11–15] A higher CO_2 conversion is usually achieved in the olefin intermediate route compared to the oxygenated intermediate route, which means higher space-time yields for gasoline (STY_{GL}, moles of CO_2 converted to gasoline per gram of iron per second).[9,16]

In the olefin intermediate route, CO_2 was first reduced to CO by the reversed water gas shift (RWGS) reaction and the generated CO was hydrogenated to an olefin intermediate by the Fischer–Tropsch synthesis (FTS) reaction, and then converted to gasoline on acidic zeolites.[17,18] Therefore, it is very crucial to first convert CO_2 to olefins with high selectivity. Among the many modified CO_2 Fischer–Tropsch synthesis (CO_2-FTS) catalysts (Fe, Co, Ni, Pt, and Cu),[19,20] iron-based catalysts have been widely considered the preferred catalyst for the CO_2-FTS process due to their excellent catalytic ability for RWGS and FTS reactions, low cost and resistance to sulfur poisoning.[21,22] Iron species undergo carburization and oxidation reactions to form Fe_3O_4 and χ-Fe_5C_2 phases during the CO_2 hydrogenation reaction. Among them, Fe_3O_4 has been experimentally demonstrated to be the active phase of the RWGS. Moreover, density functional theory calculations also show that the Fe_3O_4 (111) surface is very active in CO_2.[23] The χ-Fe_5C_2 species is widely regarded as the active phase of the FTS reaction to catalyze CO activation and C–C coupling. Moderately increasing the content of the χ-Fe_5C_2 phase in the catalyst is beneficial for the formation of light olefins. For example, it has been reported that Na additives could promote carburization to convert more iron species into the χ-Fe_5C_2 phase, resulting in higher olefin selectivity.[24] Inhibition of χ-Fe_5C_2 oxidation by constructing hydrophobic shell protection has also been shown to increase the selectivity of olefins in the product.[25]

[a]*CAS Key Laboratory of Renewable Energy, Guangzhou Institute of Energy Conversion, Chinese Academy of Sciences, Guangzhou 510640, China. E-mail: wangcg@ms.giec.ac.cn*

[b]*Key Laboratory of Energy Thermal Conversion and Control of Ministry of Education, School of Energy and Environment, Southeast University, Nanjing 210096, China. E-mail: zhangqiseu@seu.edu.cn*

[c]*University of Chinese Academy of Sciences, Beijing 100049, China*

† Electronic supplementary information (ESI) available. See DOI: https://doi.org/10.1039/d2se01567f

Zeolites were widely used in oligomerization/aromatization/isomerization reactions of hydrocarbons because of their unique shape selectivity and acidity.[9,26] Among them, HZSM-5 (5.1 Å × 5.5 and 5.3 Å × 5.6 Å) with a three-dimensional pore structure had been shown to be more favorable for gasoline generation.[17] Combining the iron-based CO_2-FTS catalyst with HZSM-5 to form a tandem catalyst could shift the product distribution to the gasoline hydrocarbon range. For example, the stable production of CO_2 to gasoline could be achieved by coupling Na/Fe_3O_4 and HZSM-5, and the space-time yield of gasoline could reach 2.5 $\mu mol_{CO_2}\ g_{Fe}^{-1}\ s^{-1}$.[17] The coupling of K-ion exchanged ZSM-5 with the Fe/C–K catalyst could also catalyze the hydrogenation of CO_2 to C_5^+ products with a space time yield of 8.1 $\mu mol_{CO_2}\ g_{Fe}^{-1}\ s^{-1}$ and a catalyst lifetime of 50 hours.[27] Coupling hollow HZSM-5 with Na–Fe@C catalysts also enabled efficient preparation of gasoline from CO_2 hydrogenation, but unfortunately the life of the catalyst was still only 60 hours.[28] Although great efforts had been made in the development of composite catalysts, the space-time yield of gasoline remained low due to the poor matching between the components of the composite catalysts, and the stability of the catalysts remained to be improved. Consequently, there is an urgent need for environmentally friendly and inexpensive methods for the synthesis of highly active and stable catalysts.

Recently, we have developed a simple, stable, green, and inexpensive Fe/C catalyst synthesis process that showed high space-time yields of light olefins from CO_2.[29] If coupled with acidic HZSM-5 zeolite, it shows promise to improve the space-time yield of gasoline from CO_2. Herein, we showed that Fe/C and HZSM-5 (160) (SiO_2/Al_2O_3 molar ratio = 160) tandem catalysts with double-layer mode showed high activity and stability in the conversion of CO_2 to gasoline. The structure-activity relationships of the catalysts were also explored and revealed through a series of detailed characterization of the catalysts. Finally, we also investigated the stability of the catalyst to prove its potential value in industrial application, which made it possible to prepare simple and efficient catalysts for CO_2 hydrogenation to gasoline in the near future.

2. Experimental section

2.1 Materials

Pomelo peel (PP) was collected from a local market. $Fe(NO_3)_3 \cdot 9H_2O$ (98.5%) was purchased from Shanghai Macklin Biochemical Co., Ltd. HZSM-5 (SiO_2/Al_2O_3 = 50, 160, 300) from Nankai University Catalyst Company was calcined at 500 °C in air for 4 h before use.

2.2 Catalyst preparation

The white inner skin of PP was cut into fine strips and then dried in a vacuum freeze dryer to remove moisture. The dried PP was crushed into powder for further use. Typically, 6 g of PP was impregnated with 45 mL of aqueous iron nitrate solution (8×10^{-3} g mL^{-1}) and stirred at 50 °C for 10 hours. Then, the samples were dried in an oven at 100 °C for 10 h. Finally, the dried samples were crushed and pyrolyzed in a stream of N_2 at 400 °C for 3 h. The actual loading of Fe in the samples was measured by ICP-OES to be 14.0 wt%.

2.3 Catalyst characterization

The crystal structures of the powder samples were examined by powder X-ray diffraction (XRD, X'Pert Pro MPD with Cu Kα radiation, $\lambda = 0.154$ nm, the scanning angle 2θ = 5–80°, Philips, the Netherlands). Transmission electron microscopy (TEM) images were obtained on a JEOL-2100F with 200 kV accelerating voltage. The specific surface area of the catalysts was analyzed by the BET method by carrying out N_2 adsorption measurements at −196 °C on a Micromeritics Gemini VII 2390 instrument. Then, NH_3-TPD was carried out in a constant flow of high purity N_2 (40 mL min^{-1}) from 100 °C to 800 °C at a heating rate of 10 °C min^{-1}. The desorbed NH_3 during the heating process was detected using a thermal conductivity detector (TCD). The ^{57}Fe Mössbauer spectrum was recorded on a Topologic Systems MFD-500AV with a Co γ-quantum source in an Rh matrix at room temperature. The isomer shift (IS) value was set with respect to that of α-Fe. The obtained spectra were fitted by Lorentzian curves with a least-squares fitting procedure. Thermogravimetric analysis (TG) was carried out from 50 °C to 800 °C at a heating rate of 10 °C min^{-1} in flowing air.

2.4 Catalytic reaction

Catalytic reactions were performed in a fixed-bed reactor with an inner diameter of 8.0 mm. Before the reaction, the catalyst was *in situ* reduced at 400 °C in a pure H_2 atmosphere with a flow of 30 mL min^{-1} for 4 h at atmospheric pressure. After reduction, the reactor was cooled to 150 °C, and a mixture of gas (73% H_2/24% CO_2/3% N_2) was fed into the reactor. The tail gas was analyzed using on-line gas chromatographs (GC7890B, Agilent) equipped with thermal conductivity detectors (TCDs) and a flame ionization detector (FID). The oil product was gathered using a cold trap and analyzed using an off-line gas chromatograph (GC2010, Shimadzu) equipped with an FID and a PONA capillary column. The product selectivity was analyzed on a carbon basis, and the time-on-stream was 24 h. The carbon balances of the CO_2-FTS products in all catalytic runs were above 95%.

3. Results and discussion

3.1 Textural properties and XRD results

Fig. 1a shows the TEM photograph of Fe/C, and it could be found that the nanoparticles with an average particle size of 3.6 nm were uniformly distributed on the support, and the (220) and (311) crystalline surfaces attributed to the Fe_3O_4 phase could be observed in the high-resolution electron microscopy images. The phase structure of the catalysts was further analyzed by XRD (Fig. 1d), and the XRD pattern showed diffraction peaks at 2θ with 30.0°, 35.4°, 43.0°, 53.4°, 57.0° and 62.5° attributed to face-centered cubic Fe_3O_4 (JCPDS 19-0629), confirming the formation of Fe_3O_4 nanoparticles. The diffraction peaks of the zeolite HZSM-5(160) sample were fully correlated with the typical structure of the MFI topology.

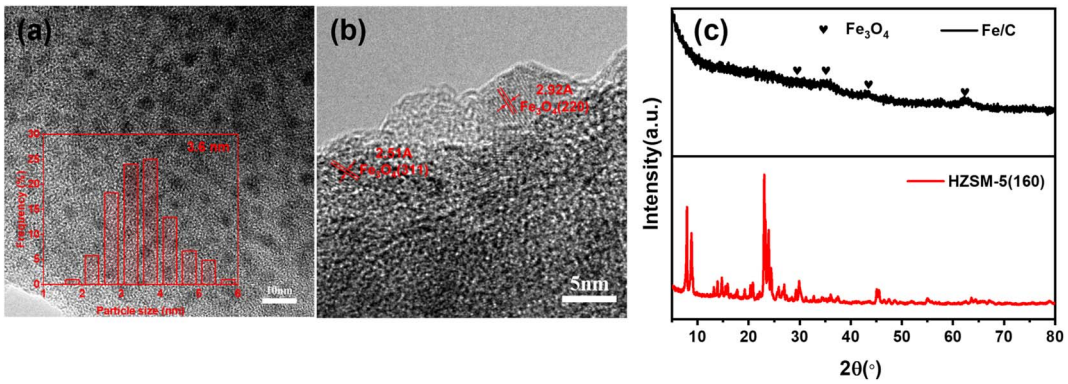

Fig. 1 TEM (a) and HRTEM (b) images of the fresh Fe/C catalyst. (c) XRD patterns of fresh Fe/C and HZSM-5(160).

3.2 Effect of HZSM-5 on product distribution

Fig. 2 compares the product distribution on Fe/C catalysts without and with HZSM-5(160) under the same reaction conditions. As shown in Fig. 2a, the selectivity and space-time yield of C_2–$C_4^=$ with 58.0% and 30.5 $\mu mol_{CO_2}\ g_{Fe}^{-1}\ s^{-1}$ could be obtained on a single Fe/C catalyst, where the selectivity and space-time yield of gasoline were 18.0% and 9.5 $\mu mol_{CO_2}\ g_{Fe}^{-1}\ s^{-1}$. Thereinto, the high space velocity was conducive to the formation of light olefins.[29] The chain growth factor (α) of hydrocarbons was 0.55. When HZSM-5(160) was added downstream of the Fe/C catalyst, the product distribution changed significantly (Fig. 2b). Among them, the most significant changes were the distribution of gasoline hydrocarbons and light olefins. The increase of gasoline hydrocarbons was at the expense of light olefins, which clearly demonstrated the oligomerization, isomerization and aromatization of olefins. In comparison, the α value on the Fe/C|HZSM-5 catalyst was 0.63, which was higher than that on the Fe/C catalyst, indicating that the multi-functional catalyst was more conducive to the formation of long-chain hydrocarbons. The selectivity and space-time yield of gasoline hydrocarbons reached 53.2% and 30.6 $\mu mol_{CO_2}\ g_{Fe}^{-1}\ s^{-1}$, respectively. In addition, the products on the multifunctional catalyst seriously deviated from the typical ASF distribution, which was attributed to the secondary reactions of oligomerization, isomerization and aromatization of olefins on the acid sites of HZSM-5(160).

To prove the pathway of oligomerization, isomerization and aromatization reactions of olefins occurring over Fe/C|HZSM-5(160) series catalysts, propylene was used directly as a reactant under the same reaction conditions described above. As expected, propylene could be converted almost completely to gasoline by oligomerization with a selectivity of 74.8%. Moreover, there are a large number of isoparaffins and aromatics in gasoline, which also proved the occurrence of olefin aromatization and isomerization reactions (Table 1).

3.3 Effect of proximity

It was reported that the proximity of two components in a tandem catalyst had an important influence on the catalytic activity as well as the product distribution.[30,31] In the selective hydrogenation of CO_2 to gasoline, it was found that the control of the proximity of tandem catalysts was also crucial. In our case, with an increase in the proximity of the two components in the tandem catalyst, the CO_2 conversion and the space-time yield of gasoline gradually decreased, while the selectivity of CO and light olefins gradually increased (Fig. 3b). This was due to the increased mutual toxic interaction between the zeolite and iron species as the proximity of the tandem catalyst increased. The acidic sites of the zeolite could reduce the surface alkalinity and carburization of the iron-based catalyst,[17] thereby reducing FTS activity, while basic sites on iron-based catalysts could also reduce the amount of acid in the adjacent

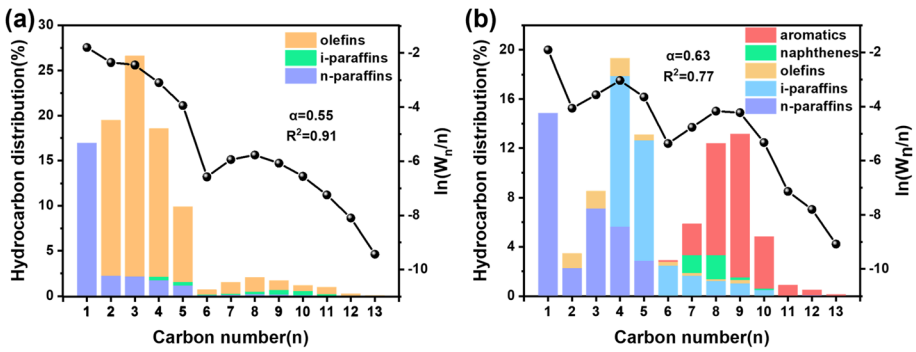

Fig. 2 Effect of HZSM-5 on product distribution: (a) over the Fe/C catalyst alone and (b) over the Fe/C|HZSM-5(160) catalyst. Reaction conditions: 0.2 g of Fe/C and 0.4 g of HZSM-5(160), 320 °C, $H_2/CO_2 = 3$, 2 MPa, GHSV = 4000 mL $h^{-1}\ g_{cat}^{-1}$, and TOS = 24 h.

Table 1 Oligomerization, isomerization and aromatization of propylene over the Fe/C|HZSM-5(160) catalyst[a]

C_3H_6 conversion (%)	Selectivity in hydrocarbons (%)			Composition in C_5–C_{11} (%)				
	$C_2^=$, $C_4^=$	C_2^0–C_4^0	C_5–C_{11}	*n*-Paraffins	i-Paraffins	Olefins	Naphthenes	Aromatics
98.5	1.6	23.6	74.8	5.4	24.5	21.9	8.4	39.8

[a] Reaction conditions: 0.2 g of Fe/C and 0.4 g of HZSM-5(160), 320 °C, $H_2/CO_2 = 3$, 2 MPa, GHSV = 4000 mL h^{-1} g_{cat}^{-1}, and TOS = 24 h.

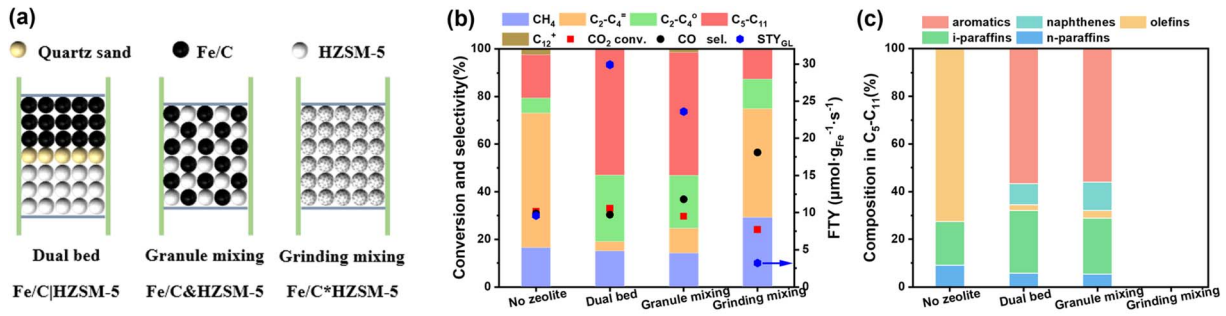

Fig. 3 Effect of the proximity of Fe/C and HZSM-5(160) on the performance of CO_2 hydrogenation. Reaction conditions: 0.2 g of Fe/C and 0.4 g of HZSM-5(160), 320 °C, 2 MPa, $H_2/CO_2 = 3$, GHSV = 4000 mL h^{-1} g_{cat}^{-1}, and TOS = 24 h.

zeolite, thereby inhibiting the oligomerization, isomerization and aromatization reactions of light olefins.[32] There was no mutual interference between the two components in a tandem catalyst with a dual-bed, so the light olefins generated on the Fe/C catalyst could be converted into long chain hydrocarbons at the acidic sites of HZSM-5 through oligomerization, isomerization and aromatization. Moreover, the proximity of the tandem catalyst could also adjust the composition of gasoline. More aromatics and isoparaffins tended to be produced in the dual-bed configuration, whereas almost no oil phase product was produced in the grinding mixing mode (Fig. 3c).

3.4 Effect of acidity

The effect of SiO_2/Al_2O_3 (50, 160 and 300) of HZSM-5 on the reaction performance was examined. The intensity of the acid sites in HZSM-5 was characterized by NH_3-TPD, as shown in Fig. 4a and Table 2. HZSM-5(50) showed two broad desorption peaks in the regions of 195 °C and 414 °C, which corresponded to the weak and strong acid sites, respectively.[33] At the same time, the desorption peaks are shifted to lower temperatures with increasing SiO_2/Al_2O_3 of HZSM-5. It indicated that increasing SiO_2/Al_2O_3 weakened the adsorption capacity of the acid sites, shifting the desorption peaks of NH_3 species to lower temperatures. In addition, the peak areas of weak and strong acid sites in the HZSM-5 catalyst showed a decreasing trend with the increasing SiO_2/Al_2O_3 ratio, indicating that the higher SiO_2/Al_2O_3 of HZSM-5 weakened the number of weak and strong acid sites. The highest gasoline selectivity was achieved over a SiO_2/Al_2O_3 of 160. Reducing or increasing the ratio would reduce the gasoline selectivity (Fig. 4b). Strong acidity of HZSM-5(50) would lead to excessive cracking of heavy hydrocarbons into C_1–C_4 hydrocarbons, while weak acidity of HZSM-5(300) was not conducive to the oligomerization, isomerization and

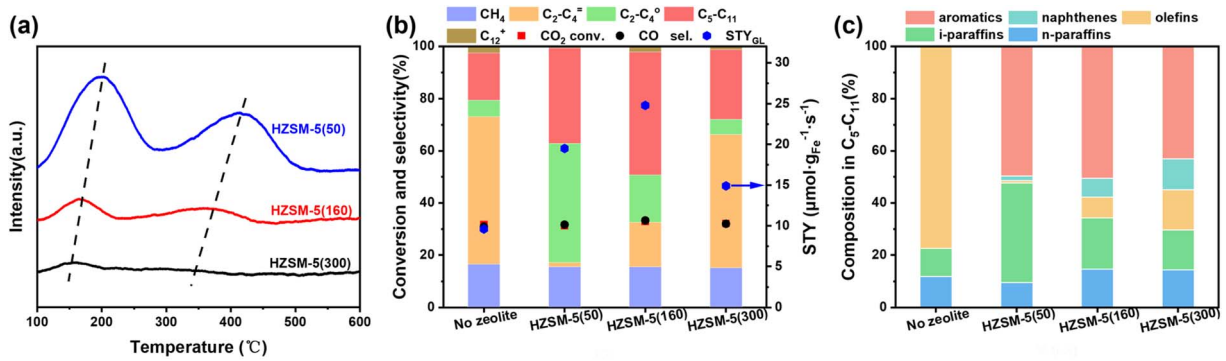

Fig. 4 Effect of acidity on the CO_2 hydrogenation performance over the Fe/C|HZSM-5 catalyst. Reaction conditions: 0.2 g of Fe/C and 0.4 g of HZSM-5, 320 °C, 2 MPa, $H_2/CO_2 = 3$, GHSV = 4000 mL h^{-1} g_{cat}^{-1}, and TOS = 24 h.

Table 2 The BET surface areas and acidic properties of the HZSM-5 zeolites

		Weak acids [b]		Strong acids [b]	
Zeolite	S_{BET} [a] ($m^2\ g^{-1}$)	Peak temperature (°C)	Acid amount ($\mu mol\ g^{-1}$)	Peak temperature (°C)	Acid amount ($\mu mol\ g^{-1}$)
HZSM-5(50)	350	194.9	423.1	413.8	268.9
HZSM-5(160)	355	165.2	181.6	363.9	80.7
HZSM-5(300)	356	159.2	84.8	300.2	16.4

[a] estimated by N_2 physisorption. [b] estimated by NH_3-TPD.

aromatization of light olefins, so they are not conducive to the selective generation of gasoline. At the same time, the SiO_2/Al_2O_3 of HZSM-5 also has a significant modulating effect on the distribution of oil phase products, with lower SiO_2/Al_2O_3 of HZSM-5 being more favorable to the formation of isoparaffins and aromatics (Fig. 4c).

3.5 Effect of reaction conditions

3.5.1 Fe/C to HZSM-5(160) mass ratio. Fig. 5a shows the effect of the Fe/C to HZSM-5(160) mass ratio on converting CO_2 to gasoline. With the increase of HZSM-5(160) addition, the selectivity and space-time yield of gasoline first increased and then decreased slightly. The selectivity of light olefins showed a downward trend. When the mass ratio of Fe/C to HZSM-5 (160) was 1 : 1, the contact time between olefins and HZSM-5 (160) was short, which could not meet the oligomerization, isomerization and aromatization of light olefins. When the mass ratio of Fe/C to HZSM-5(160) reached 1 : 3, more light olefins were converted, but the selectivity of gasoline did not further improve, and the selectivity of light alkanes increased slightly. This was due to the fact that the prolonged contact time increased the chance of C_5–C_{11} cleavage and thus decreases its selectivity in the final products.

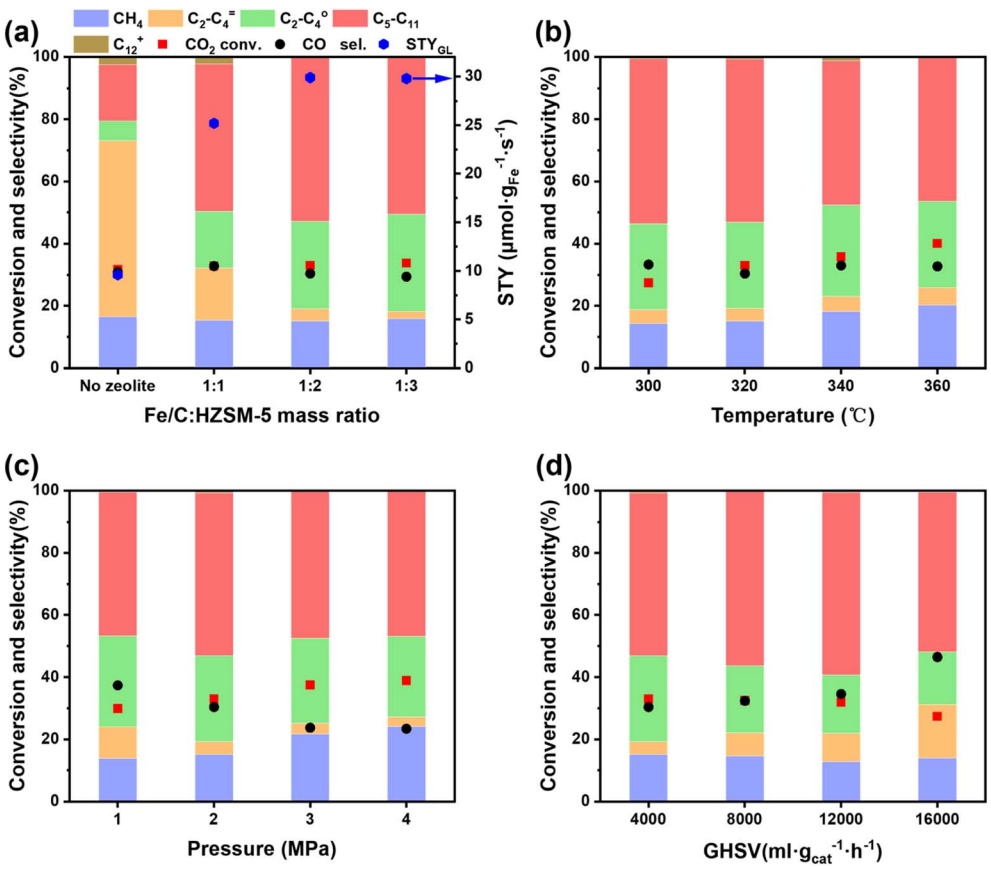

Fig. 5 The performance of the Fe/C|HZSM-5(160) catalyst under different conditions: (a) Fe/C to HZSM-5 mass ratio (0.2 g of Fe/C and 0.2, 0.4, and 0.6 g of HZSM-5, 320 °C, 2 MPa, 40 mL min^{-1}). (b) Temperature (0.2 g of Fe/C and 0.4 g of HZSM-5, 2.0 MPa, GHSV = 4000 mL $g_{cat}^{-1}\cdot h^{-1}$). (c) Pressure (0.2 g of Fe/C and 0.4 g of HZSM-5, 320 °C, GHSV = 4000 mL $g_{cat}^{-1}\cdot h^{-1}$); (d) GHSV (0.2 g of Fe/C and 0.4 g of HZSM-5, 320 °C, 2.0 MPa).

3.5.2 Reaction temperature. The process of CO_2 hydrogenation to gasoline involved multi-step cascade reactions, and the optimal temperature for different reactions might be different, so it was critical to select the appropriate reaction temperature to achieve a good temperature match for the multi-step reactions to improve the performance of the CO_2 hydrogenation reaction. To this end, we investigated the effect of reaction temperature on the performance of CO_2 hydrogenation over the Fe/C|HZSM-5(160) catalyst, and the results are shown in Fig. 5b. As could be seen, the CO_2 conversion gradually increased from 27.4% to 40.1%, the selectivity of CH_4 gradually increased, and the selectivity of gasoline gradually decreased from 53.0% to 46.2% as the reaction temperature increased. This indicated that increasing temperature was beneficial for CO_2 activation and hydrogenation, but excessively high temperature favored methanation rather than the C–C coupling reaction. On balance, 320 °C was a more suitable reaction temperature for this tandem catalytic reaction system.

3.5.3 Reaction pressure. The RWGS reaction was an isochoric reaction, and the FT synthesis reaction was a volume decreasing reaction. Therefore, the total reaction of CO_2 hydrogenation to gasoline belonged to a volume decreasing reaction. Increasing the pressure facilitated the forward reaction, but also made the desorption of the reaction products on the catalyst surface difficult. Therefore, appropriate reaction pressure was of great significance to improve the selectivity of gasoline. Fig. 5c shows the effect of reaction pressure on the CO_2 hydrogenation performance of the Fe/C|HZSM-5(160) catalyst. With an increase in reaction pressure, the conversion of CO_2 increased and the selectivity of CO decreased, which was because the higher pressure favored the FTS reaction and accelerated the conversion of CO intermediates, thus shifting the RWGS reaction equilibrium in a positive direction. Reaction pressure also had a significant influence on hydrocarbon product distribution. With an increase in reaction pressure, the selectivity of C_2–C_4 gradually decreased, and the selectivity of gasoline showed a trend of increasing and then decreasing, which indicated that an appropriate increase of reaction pressure was beneficial for the C–C coupling reaction, but too high a pressure could also lead to excessive hydrogenation to methane. Therefore, the optimal reaction pressure selected in the process of CO_2 hydrogenation to gasoline was 2 MPa.

3.5.4 GHSV. Fig. 5d shows the effect of GHSV on the CO_2 hydrogenation performance of the Fe/C|HZSM-5(160) catalyst. With an increase in GHSV, the CO_2 conversion gradually decreased, and the change in CO selectivity was the opposite. This was because the increase in GHSV led to a shorter contact time for various reactants on the catalyst surface, which was not conducive to the activation and dissociation of reactant molecules on the catalyst surface, resulting in a decrease in reaction activity. It was noteworthy that the selectivity of light olefins gradually increased with increasing GHSV, while the selectivity of gasoline first gradually increased and then decreased. This was because the oligomerization and direct hydrogenation of light olefins were carried out simultaneously, and the two reactions together determine the selectivity of gasoline. Moreover, the space-time yield of gasoline increased first and then decreased with the increase in GHSV. When the GHSV was 12 000 mL $g_{cat}^{-1}\cdot h^{-1}$, the selectivity and space-time yield reached the highest (58.6% and 91.2 $\mu mol_{CO_2}\ g_{Fe}^{-1}\ s^{-1}$), respectively. This result has some advantages over some of the reported iron space time yields for gasoline on catalysts (Table S1†).

3.5.5 Stability. The stability of Fe/C|HZSM-5(160) with a dual-bed configuration was also tested (Fig. 6a). It showed good stability for over 180 h on stream. Both CO_2 conversion and the selectivity of gasoline were stable at 32% and 53%, respectively. The carbon deposition of the HZSM-5 catalyst during the stability test was quantified by thermogravimetric (TG) analysis (Fig. 6b). The weight loss areas before and after 300 °C in the TG curve are related to water evaporation and char combustion,[34] respectively. The total amount of coke deposition on HZSM-5 during the stability test was only 3.9 wt%, which resulted in the excellent stability of the tandem catalyst.[11] Therefore, this green, cheap tandem catalyst showed great potential in the large-scale application of CO_2 hydrogenation to gasoline.

3.6 Reaction scheme for CO_2 hydrogenation

In order to investigate the reaction pathway of CO_2 hydrogenation to gasoline over this tandem catalyst, the iron phase composition of the spent catalyst was analyzed using the ^{57}Fe Mössbauer spectrum. As shown in Fig. 7, the iron phase in Fe/C after 24 h of reaction included 22.3% Fe_3O_4 and 50.8% Fe_5C_2, which were the active phases of the RWGS reaction and FTS reaction, respectively. At the same time, HZSM-5 (160) was proved to have moderate acidic sites by NH_3-TPD, which could catalyze oligomerization, isomerization and aromatization of light olefins.

Based on the above results, the reaction scheme of CO_2 hydrogenation to gasoline over the Fe/C|ZSM-5 tandem catalyst

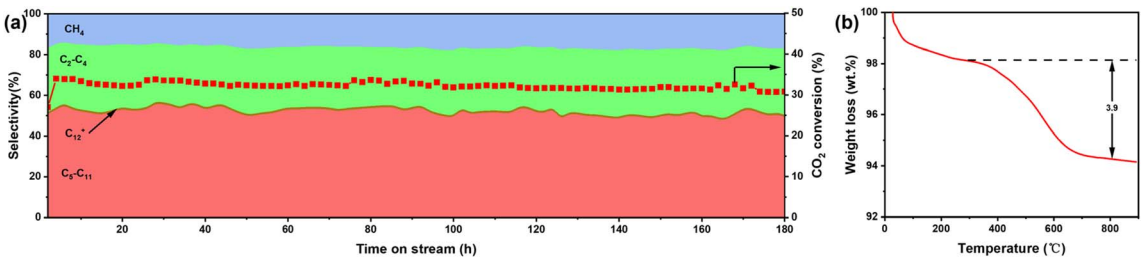

Fig. 6 Stability of the Fe/C|HZSM-5(160) catalyst. Reaction conditions: 0.2 g of Fe/C and 0.4 g of HZSM-5(160), 320 °C, $H_2/CO_2 = 3$, 2 MPa, GHSV = 4000 mL h^{-1} g_{cat}^{-1}, and TOS = 180 h.

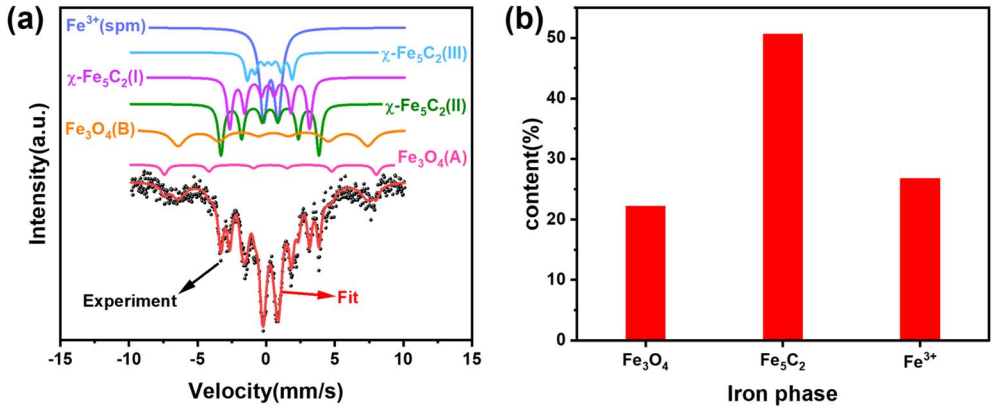

Fig. 7 (a) ^{57}Fe Mössbauer spectrum and fitted subspectra. (b) Composition of the iron phases in the tandem catalysts after 24 h of reaction determined by the relative absorption areas from Mössbauer spectra.

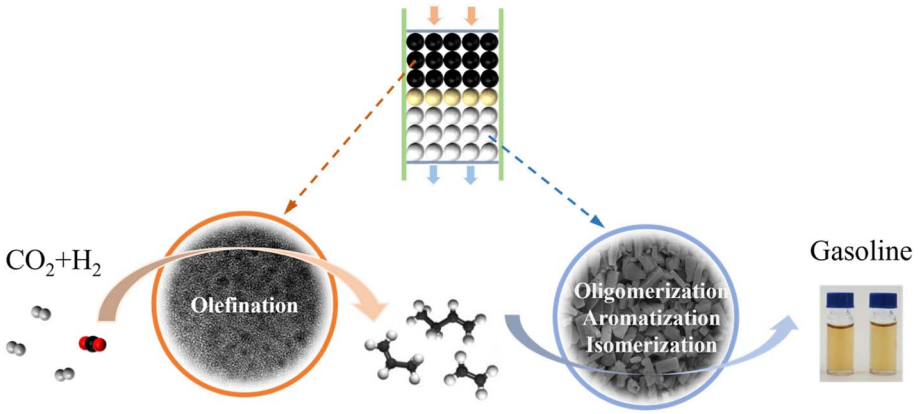

Fig. 8 Proposed reaction routes for converting CO_2 to gasoline over the tandem catalysts.

could be described as shown in Fig. 8. The scheme showed that the series of catalysts with three active sites have complementary and compatible properties. During CO_2 hydrogenation, CO_2 was first reduced to CO by H_2 on Fe_3O_4, and then CO and H_2 passed through the FTS on Fe_5C_2 to generate light olefin intermediates. The olefin intermediate diffused to the downstream acid site of HZSM-5, where acid-catalyzed reactions (oligomerization, isomerization and aromatization) occurred, resulting in the selective generation of the gasoline range of isoparaffins and aromatics. In addition, the selectivity and space-time yield of gasoline could be adjusted by varying the mass ratio of Fe/C to HZSM-5 and the way it was combined. This also demonstrated that the reactions over the versatile Fe/C|ZSM-5 catalyst involved an intermediate migration between different active sites.

4. Conclusions

In conclusion, we designed a Fe/C|HZSM-5 tandem catalyst and used it for the first time for one-step direct conversion of CO_2 to gasoline. The catalyst contained three active sites (Fe_3O_4, Fe_5C_2 and acid sites) that catalyzed the tandem reactions of RWGS, FTS and oligomerization/aromatization/isomerization. The catalytic activity of the two components of the Fe/C|HZSM-5 catalyst could be better exploited in the dual-layered filling mode, and neither too strong nor too weak an acidity of HZSM-5 was conducive to the production of gasoline. The Fe/C|HZSM-5 catalyst exhibited high gasoline selectivity (58.6%) and space-time yield (91.2 $\mu mol_{CO_2}\, g_{Fe}^{-1}\, s^{-1}$). In addition, the activity of the catalyst did not decrease in 180 h. The above findings strongly confirm the feasibility of a simple and efficient preparation of catalysts for thermo-catalytic upgrading of CO_2 to gasoline. Overall, this newly developed process has the advantages of simplicity of operation, stability, greenness, and low price, making it an efficient and industrially applicable solution.

Data availability

ESI† and the data supporting the findings of this study are available online, or from the corresponding authors upon reasonable request.

Conflicts of interest

There are no conflicts to declare.

Acknowledgements

The authors are thankful to the financial support by the National Key R&D Program of China (2022YFE0207200), the National Natural Science Foundation of China (No. 51876209), the "Transformational Technologies for Clean Energy and Demonstration", the Strategic Priority Research Program of the Chinese Academy of Sciences (No. XDA21060102), and the Key Technologies R&D Program of Guangdong Province (2020B1111570001).

References

1 W. Cramer, J. Guiot, M. Fader, J. Garrabou, J.-P. Gattuso, A. Iglesias, M. A. Lange, P. Lionello, M. C. Llasat, S. Paz, J. Peñuelas, M. Snoussi, A. Toreti, M. N. Tsimplis and E. Xoplaki, *Nat. Clim. Change*, 2018, **8**, 972–980.
2 W. M. Washington, G. A. Meehl, W. D. Collins and J. M. Arblaster, *Science*, 2005, **307**, 1769–1773.
3 S. Sun, H. Sun, P. T. Williams and C. Wu, *Sustainable Energy Fuels*, 2021, **5**, 4546–4559.
4 S. Kirsch, *Extr. Ind. Soc.*, 2020, **7**, 838–840.
5 M. D. Porosoff, B. Yan and J. G. Chen, *Energy Environ. Sci.*, 2016, **9**, 62–73.
6 W. Zhou, K. Cheng, J. Kang, C. Zhou, V. Subramanian, Q. Zhang and Y. Wang, *Chem. Soc. Rev.*, 2019, **48**, 3193–3228.
7 R. P. Ye, J. Ding, W. Gong, M. D. Argyle, Q. Zhong, Y. Wang, C. K. Russell, Z. Xu, A. G. Russell, Q. Li, M. Fan and Y. G. Yao, *Nat. Commun.*, 2019, **10**, 5698.
8 J. Yang, X. Pan, F. Jiao, J. Li and X. Bao, *Chem. Commun.*, 2017, **53**, 11146–11149.
9 P. Gao, S. Li, X. Bu, S. Dang, Z. Liu, H. Wang, L. Zhong, M. Qiu, C. Yang, J. Cai, W. Wei and Y. Sun, *Nat. Chem.*, 2017, **9**, 1019–1024.
10 K. Cheng, W. Zhou, J. Kang, S. He, S. Shi, Q. Zhang, Y. Pan, W. Wen and Y. Wang, *Chem*, 2017, **3**, 334–347.
11 J. Wei, R. Yao, Q. Ge, Z. Wen, X. Ji, C. Fang, J. Zhang, H. Xu and J. Sun, *ACS Catal.*, 2018, **8**, 9958–9967.
12 J. Wei, R. Yao, Y. Han, Q. Ge and J. Sun, *Chem. Soc. Rev.*, 2021, **50**, 10764–10805.
13 X. Yang, G. Song, M. Li, C. Chen, Z. Wang, H. Yuan, Z. Zhang and D. Liu, *Ind. Eng. Chem. Res.*, 2022, **61**, 7787–7798.
14 Z. Shi, H. Yang, P. Gao, X. Chen, H. Liu, L. Zhong, H. Wang, W. Wei and Y. Sun, *Chin. J. Catal.*, 2018, **39**, 1294–1302.
15 L. Zhang, Y. Dang, X. Zhou, P. Gao, A. Petrus van Bavel, H. Wang, S. Li, L. Shi, Y. Yang, E. I. Vovk, Y. Gao and Y. Sun, *Innovation*, 2021, **2**, 100170.
16 S. De, A. Dokania, A. Ramirez and J. Gascon, *ACS Catal.*, 2020, **10**, 14147–14185.
17 J. Wei, Q. Ge, R. Yao, Z. Wen, C. Fang, L. Guo, H. Xu and J. Sun, *Nat. Commun.*, 2017, **8**, 15174.
18 A. Noreen, M. Li, Y. Fu, C. C. Amoo, J. Wang, E. Maturura, C. Du, R. Yang, C. Xing and J. Sun, *ACS Catal.*, 2020, **10**, 14186–14194.
19 Z. Shi, H. Yang, P. Gao, X. Li, L. Zhong, H. Wang, H. Liu, W. Wei and Y. Sun, *Catal. Today*, 2018, **311**, 65–73.
20 R. Satthawong, N. Koizumi, C. Song and P. Prasassarakich, *J. CO_2 Util.*, 2013, **3–4**, 102–106.
21 B. Hu, S. Frueh, H. F. Garces, L. Zhang, M. Aindow, C. Brooks, E. Kreidler and S. L. Suib, *Appl. Catal., B*, 2013, **132–133**, 54–61.
22 S. Saeidi, S. Najari, F. Fazlollahi, M. K. Nikoo, F. Sefidkon, J. J. Klemeš and L. L. Baxter, *Renewable Sustainable Energy Rev.*, 2017, **80**, 1292–1311.
23 T. Su, Z. Qin, G. Huang, H. Ji, Y. Jiang and J. Chen, *Appl. Surf. Sci.*, 2016, **378**, 270–276.
24 B. L. Liang, H. M. Duan, T. Sun, J. Ma, X. Liu, J. Xu, X. Su, Y. Huang and T. Zhang, *ACS Sustainable Chem. Eng.*, 2018, **7**, 925–932.
25 Y. F. Xu, X. Y. Li, J. H. Gao, J. Wang, G. Ma, X. Wen, Y. Yang, Y. Li and D. Mingyue, *Science*, 2021, **371**, 1–4.
26 C. Wen, K. Jin, L. Lu, Q. Jiang, J. Wu, X. Zhuang, X. Zhang, L. Chen, C. Wang and L. Ma, *Fuel*, 2023, **331**, 125855.
27 L. Guo, S. Sun, J. Li, W. Gao, H. Zhao, B. Zhang, Y. He, P. Zhang, G. Yang and N. Tsubaki, *Fuel*, 2021, **306**, 121684.
28 Y. Wang, S. Kazumi, W. Gao, X. Gao, H. Li, X. Guo, Y. Yoneyama, G. Yang and N. Tsubaki, *Appl. Catal., B*, 2020, **269**, 118792.
29 K. Jin, C. Wen, L. Chen, Q. Jiang, X. Zhuang, X. Xu, H. Wang, L. Ma, C. Wang and Q. Zhang, *Fuel*, 2023, **333**, 126412.
30 Y. Xu, J. Liu, G. Ma, J. Wang, Q. Wang, J. Lin, H. Wang, C. Zhang and M. Ding, *Mol. Catal.*, 2018, **454**, 104–113.
31 Z. Zhou and P. Gao, *Chin. J. Catal.*, 2022, **43**, 2045–2056.
32 Y. Xu, J. Liu, G. Ma, J. Wang, J. Lin, H. Wang, C. Zhang and M. Ding, *Fuel*, 2018, **228**, 1–9.
33 C. Wen, C. Wang, L. Chen, X. Zhang, Q. Liu and L. Ma, *Fuel*, 2019, **244**, 492–498.
34 Y. F. Xu, G. Y. Ma, J. Y. Bai, Y. Du, C. Qin and M. Ding, *ACS Catal.*, 2021, 4476–4485.

